STRAIGHT-IN Dual: a platform for dual, single-copy integrations of DNA payloads and gene circuits into human induced pluripotent stem cells

Albert Blanch-Asensio[1,3], Deon S. Ploessl[2], Nathan B. Wang[2], Christine L. Mummery[1,3], Kate E. Galloway[2,4,*], Richard P. Davis[1,3,4,*]

[1] Department of Anatomy and Embryology, Leiden University Medical Center, 2300RC Leiden, The Netherlands
[2] Department of Chemical Engineering, Massachusetts Institute of Technology, MA 02139 Cambridge, USA
[3] The Novo Nordisk Foundation Center for Stem Cell Medicine, reNEW, Leiden University Medical Center
[4] Senior author
*Correspondence: katiegal@mit.edu (K.E.G), r.p.davis@lumc.nl (R.P.D)

Abstract

Targeting DNA payloads into human (h)iPSCs involves multiple time-consuming, inefficient steps that must be repeated for each construct. Here, we present STRAIGHT-IN Dual, which enables simultaneous, allele-specific, single-copy integration of two DNA payloads with 100% efficiency within one week. Notably, STRAIGHT-IN Dual leverages the STRAIGHT-IN platform to allow near-scarless cargo integration, facilitating the recycling of components for subsequent cellular modifications. Using STRAIGHT-IN Dual, we investigated how promoter choice and gene syntax influences transgene silencing, and demonstrate the impact of these design features on forward programming of hiPSCs into neurons. Furthermore, we designed a grazoprevir-inducible synZiFTR system to complement the widely-used tetracycline-inducible system, providing independent, tunable, and temporally controlled expression of both transcription factors and functional reporters. The unprecedented efficiency and speed with which STRAIGHT-IN Dual generates homogenous genetically engineered hiPSC populations represents a major advancement for synthetic biology in stem cell applications and opens opportunities for precision cell engineering.

Introduction

The efficient and rapid targeted insertion of DNA payloads, such as genetic circuits, into the genome of mammalian cells remains a significant challenge. From fundamental research to *in vivo* applications and gene or cell therapy studies, targeted integration approaches have been pivotal for tasks such as establishing functional reporters and biosensors, inserting or correcting disease-causing DNA variants, generating humanized mouse models, and programming cell fate (Balmas et al., 2023; Blanch-Asensio et al., 2022; Brandão et al., 2020; Hosur et al., 2022; Low et al., 2022; Pawlowski et al., 2017; M. Zhang et al., 2021). Recently, several platforms leveraging CRISPR/Cas technology, site-specific recombinases (SSRs) or a combination of both, have been developed to facilitate these processes. For example, prime editing combined with Bxb1 recombinase can mediate inversions of genomic regions up to 40 kb, and the insertion of DNA cargoes up to 36 kb (Anzalone et al., 2022; Pandey et al., 2024; Yarnall et al., 2023). However, CRISPR/Cas approaches often suffer from off-target effects and highly variable targeting

efficiencies, necessitating the screening of numerous clones.

SSR-based methods offer an alternative approach, though require the pre-establishment of an acceptor cell line harboring a landing pad (LP) cassette (Duportet et al., 2014; Zhu et al., 2014). However, once this is established, serine and tyrosine recombinases can mediate facile integration of large DNA payloads, with several studies reporting successful integration of fragments >100 kb (Blanch-Asensio et al., 2022; Brosh et al., 2021; Mitchell et al., 2021; Pinglay et al., 2022). These methods often use positive and/or negative selection markers in the LP cassette or donor plasmids which can yield nearly homogenous cell populations with single copy integrations (Blanch-Asensio et al., 2023). Furthermore, some approaches also allow the removal of auxiliary elements, such as fluorescent reporters or selection markers associated with the LP and the donor plasmid backbone, resulting in markerless and near scarless integration of the DNA payload (Blanch-Asensio et al., 2022; Brosh et al., 2021; J. Li et al., 2020). Recently, several novel SSRs have been reported that enable DNA integration with efficiencies comparable to or exceeding established serine and tyrosine recombinases such as Bxb1 and Cre (Durrant et al., 2023; Jelicic et al., 2023). However, Bxb1 remains a preferred recombinase due to its relatively high integration efficiency (up to 30%), ability to integrate large constructs, and the absence of pseudo-*attP* and *attB* recognition sequences in the human genome, thereby minimizing off-target events.

Bxb1 mediates the irreversible recombination of *attP* and *attB* sites, generating *attR* and *attL* sites (Brown et al., 2011). For genome engineering applications, the genomically-integrated LP cassette typically contains the *attP* site while the donor plasmid carries the *attB* site, as this combination was shown to reduce off-target integrations (Pandey et al., 2024). Through mechanistic studies of Bxb1-mediated recombination, orthogonal Bxb1 *attP*/*attB* mutant sites have been engineered by altering the traditionally used central “GT” dinucleotide sequence to a “GA” dinucleotide sequence which displays similar or higher integration efficiencies with minimal crossover between both recombination sequences (Jusiak et al., 2019; Roelle et al., 2023).

While potent compared with existing methods, one limitation of most Bxb1-based LPs is their inability to integrate multiple payloads at different locations in the human genome. Although some platforms can integrate two DNA payloads (Rosenstein et al., 2024), most lack allele-specific targeting which is required for uniform integration of both payloads. Alternative integration approaches, such as cassette exchange methods that rely on two recombination sites (Matreyek et al., 2017), are relatively inefficient. In previous work, we developed a dual acceptor line in human induced pluripotent stem cells (hiPSCs) that uses both Bxb1 and ϕC31 recombinases for orthogonal integration of two donor plasmids (Blanch-Asensio et al., 2022). However, the integration efficiency of ϕC31 was much lower than that of Bxb1 (Blanch-Asensio et al., 2022; Xu et al., 2013). Moreover, the Bxb1 LP utilized blasticidin S deaminase (*BsdR*) for positive selection, but enrichment was modest, resulting in heterogenous populations of unedited acceptor hiPSCs and cells with the integrated donor plasmid (Blanch-Asensio et al., 2022).

To address these challenges, we developed STRAIGHT-IN Dual, a hiPSC acceptor line containing two orthogonal Bxb1-recognised LPs. This system enables the rapid, simultaneous, site-specific, markerless, and near-scarless integration of two independent payloads using a single recombinase (Bxb1), with 100% of the resulting hiPSCs containing both payloads. Using our system we investigated transgene silencing ,and could compare designs as well as control for the effects of the locus and adjacent transgene. Based on biophysical models of transcription (Johnstone & Galloway, 2022), we explored how gene syntax (i.e., the relative order and orientation of genes) impacts expression from the widely-used doxycycline-inducible all-in-one Tet-On 3G

system. We observed significant differences between the four syntaxes; convergent, divergent, downstream tandem and upstream tandem, with two syntaxes identified as optimal for gene coupling in the Tet-On 3G system and the forward programming of hiPSCs to neurons. Our finding has broad implications for the design of transgenic systems and applications in research areas such as cancer biology, developmental biology, and synthetic biology.

Lastly, we characterized a grazoprevir-inducible system based on synZiFTRs in hiPSCs (H.-S. Li et al., 2022). As an orthogonal small-molecule inducible system, the grazoprevir-inducible system can be combined with the Tet-On 3G system for precise and independent control of dual transgenic payloads. We demonstrate independent control of lineage-specifying transcription factors and genetically-encoded functional reporters, facilitating both forward reprogramming of hiPSCs and real-time functional recordings at desired timepoints. Taken together, STRAIGHT-IN Dual expands the potential to explore biological questions using hiPSCs, by providing a platform to readily harness the power of state-of-the-art transgenic tools.

Results

Bxb1 mediates allele-specific integration of two DNA payloads in *CLYBL*

Building upon our previously developed STRAIGHT-IN acceptor hiPSC line that contained a single LP in one allele of *CLYBL* (Blanch-Asensio et al., 2023), we targeted the unedited *CLYBL* allele to establish a dual STRAIGHT-IN acceptor hiPSC line. The original STRAIGHT-IN LP line (LU99_*CLYBL*-bxb-v2) contains a bxb1-GT *attP* site for allele-specific targeting with GT donor plasmids, as well as an excisable fluorescent reporter (*EBFP2*) driven by the PGK promoter and a selection cassette (*BleoR*) designed as a promoter trap due to the lack of an ATG initiation codon and promoter sequence. The 5' and 3' ends of the LP are flanked by two heterospecific *loxP* and *lox257* sites, enabling Cre recombinase (Cre) to excise the auxiliary sequences both 5' and 3' of the payload following integration (**Figure 1a**).

Using TALENs, we targeted a novel LP containing a bxb1-GA *attP* site into the unedited *CLYBL* allele, thereby permitting allele-specific targeting with GA donor plasmids (**Figure 1a**). This bxb1-GA LP also includes a distinct fluorescent reporter (*mScarlet*), selection cassette (*PuroR*) and heterospecific *FRT* and *F3* sites recognized by Flp recombinase. We characterized one of the resulting hiPSC clones (STRAIGHT-IN Dual) expressing mScarlet by genotyping PCR, ddPCR and Sanger sequencing, confirming a single copy of the novel LP in the previously unedited *CLYBL* allele with no mutations in the recombination sites (**Figure 1b, 1c, Supplementary Figure 1a**). Additionally, the genomic integrity and normal karyotypic status of the hiPSC line was confirmed by ddPCR and G-band karyotyping (**Supplementary Figure 1b, 1C**). The hiPSC clone also expressed pluripotency markers and could differentiate into all three germ layers (**Supplementary Figure 1d, 1e**).

Next, we designed donor plasmids containing either *attB*-GT or *attB*-GA recombination sites. In the presence of Bxb1, these donor plasmids specifically integrate into their cognate LPs – *attB*-GT into the *attP*-GT allele and *attB*-GA into the *attP*-GA allele – allowing precise allele-specific cargo integrations (**Figure 1a**). Each donor plasmid contains the hEF1a promoter sequence and an ATG initiation codon that completes the promoter trap upon integration and leads to the expression of the respective selection markers (BleoR for the GT allele, PuroR for the GA allele), conferring resistance to either zeocin or puromycin.

We evaluated the integration efficiency of the GT and GA donor plasmids into their respective LPs using ddPCR, observing comparable levels for both alleles (1.09% ± 0.21 for GT, 1.10% ± 0.02 for GA) before selection (**Figure 1d, 1e**). Remarkably, antibiotic selection resulted in almost 100% enrichment of hiPSCs containing either the GT or GA donor plasmids (95.52% ± 1.87 for GT, 99.06% ± 0.08 for GA; **Figure 1d, 1e**). To confirm allele

Figure 1

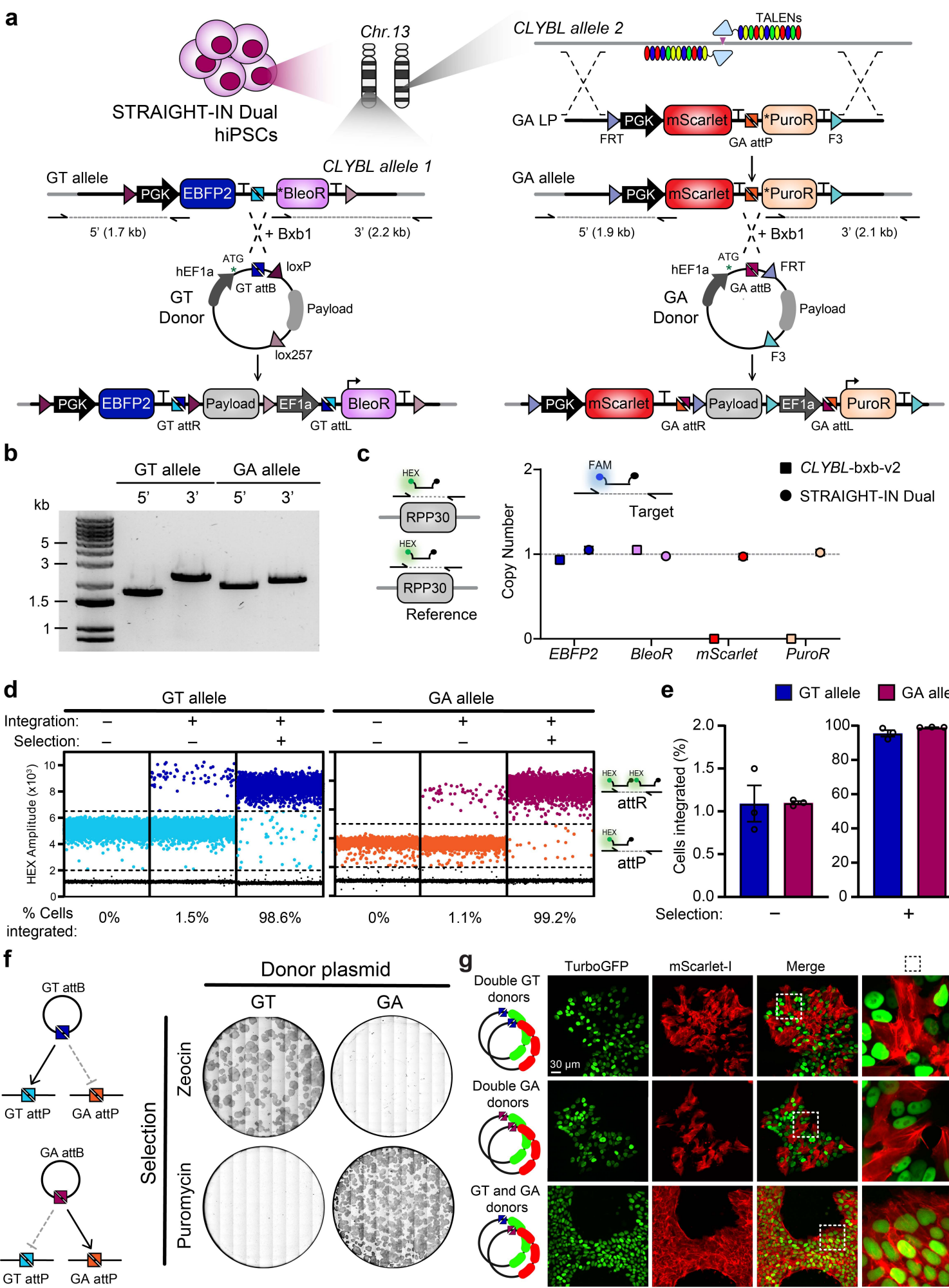
a
STRAIGHT-IN Dual hiPSCs
Chr.13
CLYBL allele 1
CLYBL allele 2
TALENs
GT allele
PGK
EBFP2
*BleoR
5' (1.7 kb)
+ Bxb1
3' (2.2 kb)
ATG
hEF1a
loxP
GT attB
GT Donor
Payload
lox257
GA LP
mScarlet
*PuroR
FRT
GA attP
F3
GA allele
5' (1.9 kb)
3' (2.1 kb)
FRT
GA attB
GA Donor
GT attR
EF1a
GT attL
GA attR
GA attL
b
GT allele
GA allele
5'
3'
kb
5
3
1.5
1
c
HEX
RPP30
Reference
FAM
Target
CLYBL-bxb-v2
STRAIGHT-IN Dual
Copy Number
EBFP2
BleoR
mScarlet
PuroR
d
Integration:
Selection:
HEX Amplitude (x10³)
attR
attP
% Cells integrated:
0%
1.5%
98.6%
1.1%
99.2%
e
Cells integrated (%)
Selection:
f
GT attB
GT attP
GA attP
GA attB
Donor plasmid
GT
GA
Selection
Zeocin
Puromycin
g
Double GT donors
Double GA donors
GT and GA donors
TurboGFP
mScarlet-I
Merge
30 µm

specificity, we separately integrated the GT and GA donor plasmids. We hypothesized that if the GT donor plasmid incorrectly integrated into the *attP*-GA LP, cells would become puromycin-resistant (**Figure 1f**). Conversely, if the GA donor plasmid integrated into the *attP*-GT LP, cells would become zeocin-resistant. Antibiotic selection for incorrect integration resulted in complete cell death, confirming the orthogonality of the alleles (**Figure 1f**). Additionally, co-transfection of both donor plasmids and a Bxb1 expression plasmid, followed by dual antibiotic selection, resulted in >93.9% of the hiPSCs containing both integrated payloads (**Supplementary Figure 2a, 2b**).

To further validate allele orthogonality, we cloned green and red fluorescent payloads (*TurboGFP* and *mScarlet-I*, respectively) into both GT and GA donor plasmids (**Figure 1g**). Additionally, *TurboGFP* was tagged with a nuclear localization sequence (NLS) and *mScarlet*-I with an actin-targeting signal to distinguish between the two payloads in individual cells. As expected, co-transfection of the fluorescent payloads targeting the same LP (either *attP*-GT or *attP*-GA) resulted in cells expressing either green or red fluorescence, but not both.

However, co-transfection of *TurboGFP*-GT and *mScarlet-I*-GA donor plasmids resulted in hiPSCs expressing both fluorescent reporters (**Figure 1g**). Furthermore, integrating the same fluorescent reporter into both LPs resulted in an ~2-fold increase in fluorescence signal, suggesting transgene expression levels are similar from both *CLYBL* alleles (**Supplementary Figure 2c**).

Accelerating and simplifying the STRAIGHT-IN Dual protocol improves cell line generation

To streamline the generation of uniform, genetically modified hiPSCs, we optimized the STRAIGHT-IN integration process to improve efficiency, increase cell yield, and shorten the timeline required to subsequently perform downstream experiments (**Figure 2a**). We hypothesized that the lower cytotoxicity and higher transgene expression typically observed with modRNA delivery compared to plasmid DNA transfection in hiPSCs, could improve integration efficiency. Transfecting modRNA encoding Bxb1 resulted in a moderate increase in integration efficiency (~2-fold) (**Supplementary Figure 2d**).

Figure 1. Targeted allele-specific integration of bxb1-GT and bxb1-GA payloads in the STRAIGHT-IN Dual hiPSC line

(a) *Schematic of TALEN-mediated targeting of the GA-LP cassette into the second allele of the citrate lyase beta-like locus (CLYBL) and Bxb1 recombinase-mediated integration of GT and GA donor plasmids into their cognate LPs. Correct donor plasmid integration activates expression of the antibiotic resistance genes in the LPs, which lack an initiation codon (*) and so are not expressed without donor plasmid integration. Half arrows indicate primer binding sites for junction PCR analysis. "Payload" indicates the location of the desired DNA cargo for targeting in both the donor plasmid and following genomic integration. "T" denotes polyadenylation sequences.*

(b) *Junction PCR analysis, using the primer pairs indicated in panel (a), confirming correct targeting of the GT and GA LPs into the CLYBL locus of the STRAIGHT-IN Dual hiPSC line.*

(c) *ddPCR validating a single copy of each LP cassette is targeted into the STRAIGHT-IN Dual hiPSC line, using the autosomal gene RPP30 (2 copy) as a reference. The hiPSC line, CLYBL-bxb-v2 (Blanch-Asensio et al., 2023), was also included as a control. Error bars show Poisson 95% CI.*

(d) *Representative ddPCR dot plots showing GT and GA donor plasmid integration before and after antibiotic selection. Dots represent droplets containing the indicated sequence (attR or attP), with percentages showing the calculated integration efficiencies.*

(e) *Mean integration efficiencies of GT and GA donor plasmids before (-) and after (+) antibiotic selection. N=3 independent transfections; error bars, ±SEM.*

(f) *Schematic of Bxb1-GT/GA recombination specificity (left), and alkaline phosphatase staining (right) showing the orthogonality of GT/GA alleles for donor plasmid integration in hiPSCs following selection.*

(g) *Fluorescence images showing that GT and GA donor plasmids expressing green (TurboGFP) or red (mScarlet-I) fluorescent payloads, respectively, integrate exclusively into their corresponding GT or GA allele.*

Next, we explored whether cytoprotective factors like p53DD could enhance the number of cells surviving post-genome modification, as has been observed for CRISPR-based genome editing (Haideri et al., 2022, 2024). Co-transfection of *p53DD* modRNA increased the fraction of cells with an integrated cargo by 12.4-fold compared to a control *mGreenLantern* modRNA (**Supplementary Figure 2e**). We also examined four Bxb1 mutants (evoBxb1, Bxb1-V74A; eeBxb1, Bxb1-V74A + E229K + V375I; Bxb1-I87L; and Bxb1-I87L + A369P + E434G), which were reported to exhibit higher recombination activity than wild-type Bxb1 (Hew et al., 2024; Pandey et al., 2024). Co-transfection of modRNAs encoding these Bxb1 variants with *p53DD* modRNA revealed that eeBxb1, in combination with p53DD, significantly increased pre-selection integration efficiency from 2.75% to 9.12% at the GT allele, and from 1.46% to 11.7% at the GA-allele (**Figure 2b**). Other Bxb1 variants did not show significant improvements, although co-transfection of *p53DD* modRNA consistently boosted integration efficiencies across all experiments (**Supplementary Figure 2f**).

To expedite enrichment using zeocin or puromycin, we utilized modRNA for faster Bxb1 expression compared to plasmid DNA. This reduced the time required to obtain uniform, payload-carrying hiPSCs to less than one week (**Figure 2c,d**). Notably, the addition of *p53DD* modRNA yielded hiPSC colonies with both GT and GA donor plasmids integrated after just 3 days of antibiotic selection (**Figure 2e**, **Supplementary Figure 2g**). ddPCR analysis confirmed single-copy integrations of the GT and GA donor plasmids, with no evidence of random integration (**Supplementary Figure 2h**).

The tyrosine recombinases, Cre and Flp, mediate the excision of the auxiliary elements following integration, resulting in a hiPSC line containing just the DNA payload and often improving the expression of the integrated transgenes (**Figure 2f**)(Blanch-Asensio et al., 2022). We sought to improve excision efficiency by testing DNA-free delivery methods for Cre and Flp using modRNA or recombinant protein, replacing traditional plasmid-based approaches. Although plasmid transfections can result in high excision efficiencies via enrichment, the selection often results in few clones surviving, leading to clonal bottlenecks and prolonged waiting times for clonal expansion.

For the GT allele, Cre protein achieved excision rates of 91.9% and 80.7% of the *loxP* and *lox257* flanked sequences, respectively, with a second Cre administration increasing this to 97.6% and 93.7% (**Figure 2g**). Since Flp protein is unavailable, we used *Flp* modRNA for excision at the GA allele. After one round of transfection, 61.5% and 54.8% of the hiPSCs had excised the *FRT* and *F3* flanked sequences, respectively, with a second transfection increasing this to 87.8% and 76.3% (**Supplementary Figure 2i**, *left*). Co-delivery of Cre protein and *Flp* modRNA resulted in 83.6% of hiPSCs excising all flanked auxiliary sequences after two transfection rounds (**Supplementary Figure 2i**, *right*).

We hypothesized that including selection during the excision process could improve efficiency as seen for integration, and potentially result in 100% of the hiPSCs excising the auxiliary sequences after a single transfection. As a proof of concept, we integrated a donor plasmid into the GA allele, conferring puromycin resistance but keeping the cells zeocin sensitive. Transfecting a modRNA encoding both Flp and BleoR (*Flp-2A-BleoR*), followed by zeocin selection, resulted in nearly complete excision of both upstream and downstream auxiliary elements within 3 days with excision rates of 99.3% and 97.2%, respectively (**Figure 2**H). Unfortunately, this strategy could not be replicated with Cre for donor plasmids integrated at the GT allele, as puromycin selection following *Cre-2A-PuroR* or *Cre-IRES-PuroR* modRNA transfection failed to yield puromycin-resistant hiPSCs (data not shown). Co-transfection of *Cre* and *PuroR* modRNAs resulted in limited excision enrichment, with efficiencies only increasing from 25.7% to 44.3% for *loxP* and from 22.5% to 41.7% for *lox257* flanked sequences, respectively (**Supplementary Figure 2j**).

Figure 2

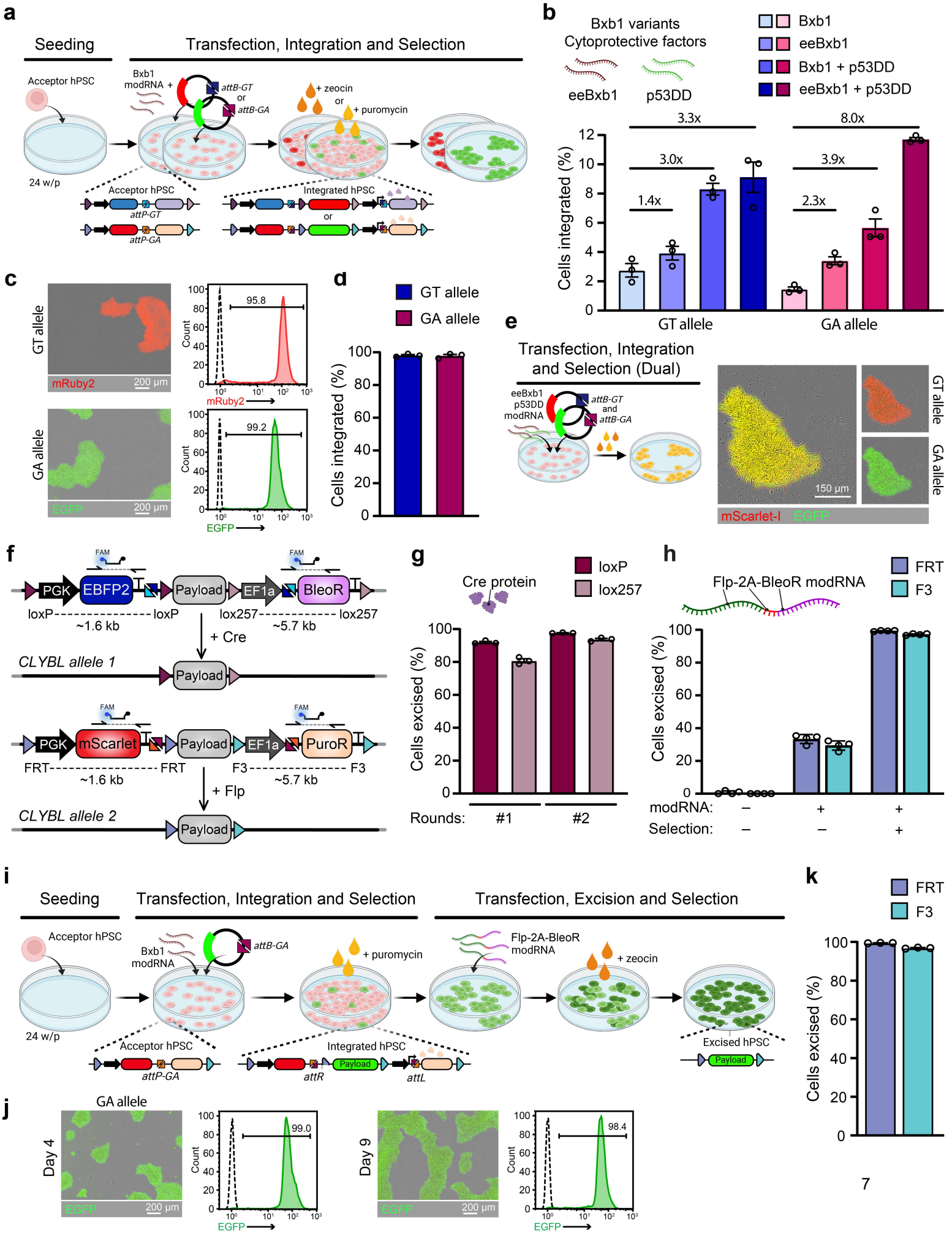
a
Seeding
Transfection, Integration and Selection
Acceptor hPSC
24 w/p
Bxb1 modRNA +
attB-GT or attB-GA
+ zeocin or + puromycin
Acceptor hPSC
attP-GT
attP-GA
Integrated hPSC
or
b
Bxb1 variants
Cytoprotective factors
eeBxb1
p53DD
Bxb1
eeBxb1
Bxb1 + p53DD
eeBxb1 + p53DD
Cells integrated (%)
3.3x
8.0x
3.0x
3.9x
1.4x
2.3x
GT allele
GA allele
c
GT allele
mRuby2
200 µm
95.8
Count
mRuby2
GA allele
EGFP
200 µm
99.2
EGFP
d
GT allele
GA allele
Cells integrated (%)
e
Transfection, Integration and Selection (Dual)
eeBxb1
p53DD
modRNA
attB-GT and attB-GA
150 µm
mScarlet-I
EGFP
GT allele
GA allele
f
FAM
PGK
EBFP2
Payload
EF1a
BleoR
loxP
loxP
~1.6 kb
lox257
lox257
~5.7 kb
+ Cre
CLYBL allele 1
Payload
PGK
mScarlet
Payload
EF1a
PuroR
FRT
FRT
~1.6 kb
F3
F3
~5.7 kb
+ Flp
CLYBL allele 2
Payload
g
Cre protein
loxP
lox257
Cells excised (%)
Rounds:
#1
#2
h
Flp-2A-BleoR modRNA
FRT
F3
Cells excised (%)
modRNA:
Selection:
i
Seeding
Transfection, Integration and Selection
Transfection, Excision and Selection
Acceptor hPSC
24 w/p
Bxb1 modRNA
attB-GA
+ puromycin
Flp-2A-BleoR modRNA
+ zeocin
Acceptor hPSC
attP-GA
Integrated hPSC
attR
Payload
attL
Excised hPSC
Payload
k
FRT
F3
Cells excised (%)
j
GA allele
Day 4
EGFP
200 µm
99.0
Count
EGFP
Day 9
EGFP
200 µm
98.4
Count
EGFP

Finally, to further streamline the workflow and eliminate the need to passage the cells, we completed the entire STRAIGHT-IN protocol – from donor plasmid integration to auxiliary element excision – within the same well. For this, we co-transfected *eeBxb1* and *p53DD* modRNA with a bxb1-GA donor plasmid containing *EGFP*, applied puromycin selection, followed by *Flp-2A-BleoR* modRNA transfection, and zeocin selection (**Figure 2i**). Within 9 days and in a single well, we achieved near uniform EGFP expression in the hiPSCs, with all auxiliary elements excised (**Figure 2j,k**), demonstrating >98% precision, markerless, and near-scarless single-copy genome integration.

The hEF1a promoter is silenced over time in hiPSCs

Transgenes have revolutionized our ability to measure cellular processes and control cell behavior and identity (Peterman et al., 2024). However, genome-integrated transgenes are prone to silencing, particularly in hiPSCs, and even more so upon differentiation. Promoter choice influences both the rate and cell-type specificity of transgene silencing (Cabrera et al., 2022; Seczynska et al., 2022). While both the CMV early enhancer/chicken β-actin (CAG) promoter and human elongation factor 1-alpha (hEF1a) promoter are known to support robust transgene expression across various cell types (Dou et al., 2021), their comparative activity in hiPSCs remains understudied.

To compare the performance of these two promoters directly, we generated a dual reporter hiPSC line with divergently oriented promoters, each driving expression of a distinct fluorescent reporter. In this line, the CAG promoter drove *mRuby2* expression and the hEF1a promoter controlled *mGreenLantern* expression. As expected, all puromycin-resistant hiPSC colonies uniformly expressed mRuby2. However, despite uniform integration of the hEF1a- *mGreenLantern* cassette, only a fraction of colonies expressed this reporter, indicating transgene silencing. This silencing became more pronounced with additional passaging of the hiPSCs (**Figure 3a**).

Figure 2. Optimized STRAIGHT-IN protocol improved integration and excision efficiencies while reducing timelines

(a) *Schematic of the STRAIGHT-IN rapid integration procedure.*

(b) *Mean integration efficiencies of GT and GA donor plasmids before antibiotic selection using combinations of Bxb1, eeBxb1 and p53DD modRNAs. N=3 independent transfections; error bars, ±SEM.*

(c) *Overlay of fluorescence and phase contrast images (left) and flow cytometric analysis (right) of hiPSCs after the STRAIGHT-IN rapid procedure using GT or GA donor plasmids carrying mRuby2 and EGFP payloads, respectively. Dashed lines represent untransfected STRAIGHT-IN Dual acceptor hiPSCs.*

(d) *Mean integration efficiencies of GT and GA donor plasmids after antibiotic selection. N=3 independent transfections; error bars, ±SEM.*

(e) *Schematic of the STRAIGHT-IN Dual rapid integration procedure with dual antibiotic selection (left), and overlay of fluorescence and phase contrast images (right) of hiPSCs after simultaneous integration of GT and GA donor plasmids carrying mScarlet-I and EGFP payloads, respectively.*

(f) *Schematic of selection cassette and plasmid backbone excision using Cre or Flp recombinases following GT or GA donor plasmid integration. Dashed lines indicate the sequences excised, and half arrows indicate the primer binding sites for ddPCR analysis.*

(g) *Mean percentages of hiPSCs with indicated flanking regions excised after 1 (#1) or 2 (#2) administrations of Cre protein, as determined by ddPCR. N=3 independent transfections; error bars, ±SEM.*

(h) *Mean percentages of hiPSCs with indicated flanking regions excised after Flp-2A-BleoR modRNA transfection, with (+) or without (-) zeocin selection, as determined by ddPCR. N=4 independent transfections; error bars, ±SEM.*

(i) *Schematic of the complete STRAIGHT-IN rapid integration/excision procedure.*

(j) *Overlay of fluorescence and phase contrast images, and flow cytometric analysis of hiPSCs on days 4 and 9 of the STRAIGHT-IN rapid integration/excision procedure transfected with a GA donor plasmid containing EGFP. Dashed lines represent untransfected STRAIGHT-IN Dual acceptor hiPSCs.*

(k) *Mean percentage of hiPSCs with indicated flanking regions excised after Flp-2A-BleoR modRNA transfection and zeocin selection, as determined by ddPCR. N=3 independent transfections; error bars, ±SEM.*

Figure 3

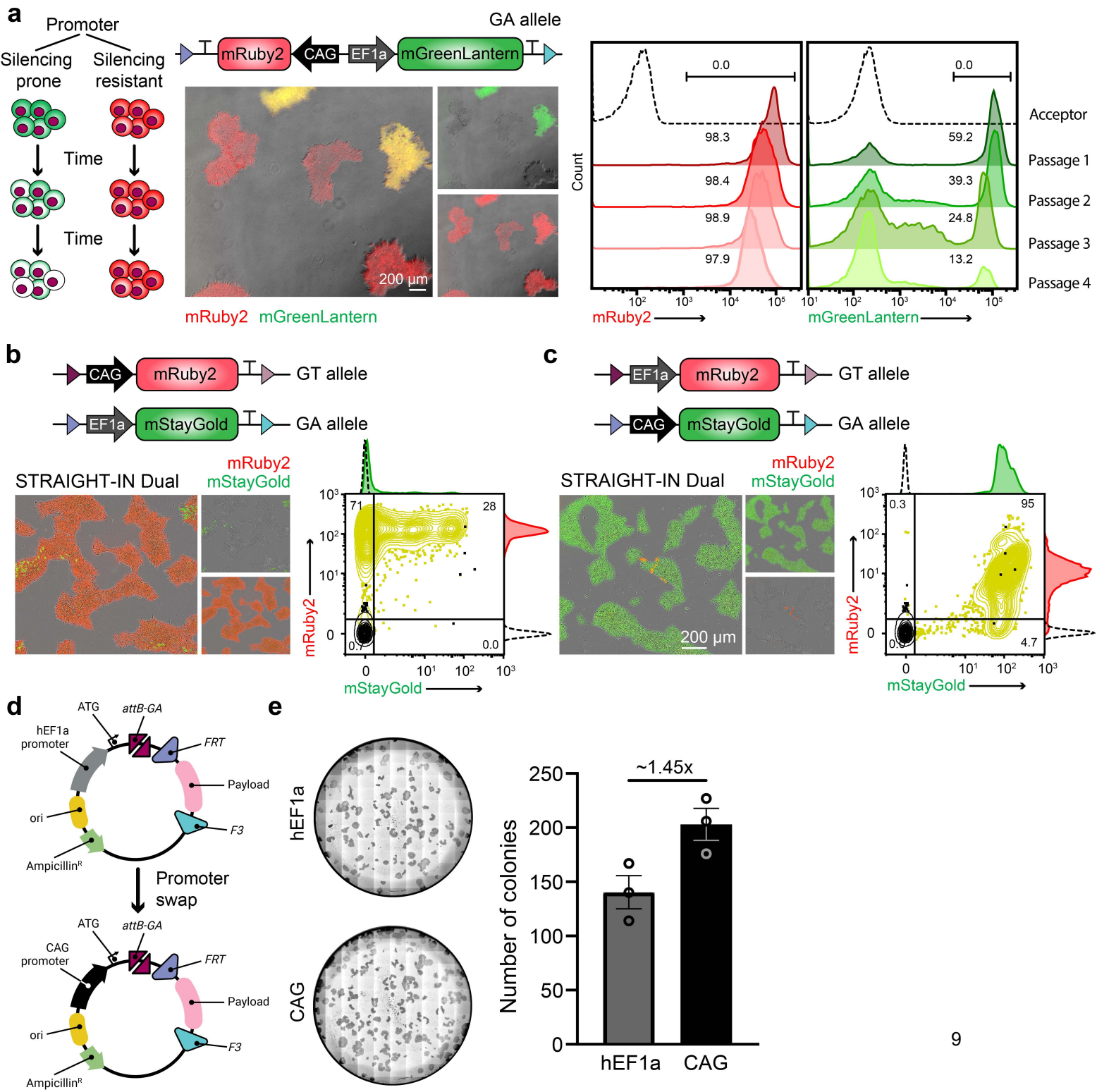
a
Promoter
Silencing prone
Silencing resistant
Time
Time
GA allele
mRuby2
CAG
EF1a
mGreenLantern
200 μm
mRuby2 mGreenLantern
Count
0.0
98.3
98.4
98.9
97.9
59.2
39.3
24.8
13.2
Acceptor
Passage 1
Passage 2
Passage 3
Passage 4
mRuby2
mGreenLantern
b
CAG
mRuby2
GT allele
EF1a
mStayGold
GA allele
STRAIGHT-IN Dual
mRuby2
mStayGold
71
28
0.7
0.0
mRuby2
mStayGold
c
EF1a
mRuby2
GT allele
CAG
mStayGold
GA allele
STRAIGHT-IN Dual
mRuby2
mStayGold
200 μm
0.3
95
0.5
4.7
mRuby2
mStayGold
d
ATG
attB-GA
hEF1a promoter
FRT
Payload
ori
F3
Ampicillin^R
Promoter swap
CAG promoter
e
hEF1a
CAG
~1.45x
Number of colonies
250
200
150
100
50
0
hEF1a
CAG

To determine whether this effect was specific to *mGreenLantern*, we replaced it with *mStayGold*, the brightest monomeric GFP currently available (H. Zhang et al., 2024). Additionally, we integrated the two reporters into separate *CLYBL* alleles to eliminate any potential interference from adjacent genes. In this configuration, only the hEF1a-driven mStayGold was silenced (**Figure 3b**). As expected, swapping the promoters resulted in strong expression of CAG-driven mStayGold, while hEF1a-driven mRuby2 was silenced, further confirming the susceptibility of the hEF1a promoter to silencing in hiPSCs (**Figure 3c**).

In our STRAIGHT-IN system, the hEF1a promoter drives *PuroR* expression in hiPSCs that have integrated the GA donor plasmid. We hypothesized that promoter silencing could be limiting the number of colonies recovered after puromycin selection. To test this, we replaced the hEF1a promoter in the GA donor plasmid with the CAG promoter (**Figure 3d**). After puromycin selection, we observed ~50% more puromycin-resistant colonies with the CAG-containing bxb1-GA donor plasmid, suggesting that silencing and/or insufficient expression of the selection cassette when under the control of the hEF1a promoter was reducing colony yield (**Figure 3e**).

Gene syntax determines induction efficiency in the Tet-On 3G system in hiPSCs

In addition to promoter selection, the relative arrangement of transcriptional units, often referred to as gene syntax, can influence the expression of adjacent genes (Engreitz et al., 2016; Johnstone & Galloway, 2022; Patel et al., 2023). While placing different elements of genetic circuits, such as inducible systems, at separate genomic loci may prevent suboptimal interactions between genes, integration at separate sites also requires integrating additional genetic cargo. To systematically compare how different designs of multi-component genetic circuits perform, we used STRAIGHT-IN Dual to elucidate key design principles, focusing on the Tet-On 3G system and examining trade-offs between co-localized and dual locus integration.

We first constructed a *trans* design of the Tet-On 3G system, with the transcriptional units integrated into the separate *CLYBL* alleles (**Figure 4a**). The inducible gene (*mScarlet*) was driven by a tetracycline response element (TRE) containing seven tetracycline operator (*TetO*) repeats. Having determined the CAG promoter resists silencing in hiPSCs, we used this promoter to drive expression of the transactivator gene *rtTA* in a bicistronic cassette which also expressed a nuclear-localized blue fluorescent reporter (*mTagBFP2-NLS)* as a proxy readout for rtTA levels.

Figure 3. Evaluation of promoter silencing using STRAIGHT-IN

(a) *Schematic illustrating the phenomena of transgene silencing over time (left), overlaid fluorescence and phase contrast images (middle), and flow cytometric analysis over 4 passages (right) of hiPSCs expressing mRuby2 and mGreenLantern reporters in cis, driven by the CAG and hEF1a promoters respectively, and integrated at the GA allele. Dashed lines represent untransfected STRAIGHT-IN Dual acceptor hiPSCs.*

(b) *Overlaid fluorescence and phase contrast images (left) and flow cytometric analysis (right) of hiPSCs expressing mRuby2 and mStayGold reporters in trans, driven by the CAG and hEF1a promoters respectively, and integrated at the GT and GA alleles. Dashed lines represent untransfected STRAIGHT-IN Dual acceptor hiPSCs.*

(c) *Overlaid fluorescence and phase contrast images (left) and flow cytometric analysis (right) of hiPSCs expressing mRuby2 and mStayGold reporters in trans, driven by the hEF1a and CAG promoters respectively, and integrated at the GT and GA alleles. Dashed lines represent untransfected STRAIGHT-IN Dual acceptor hiPSCs.*

(d) *Schematics of GA donor plasmids containing either hEF1a or CAG promoter sequences.*

(e) *Representative phase contrast images (left) of wells containing puromycin-resistant hiPSC colonies following integration of the donor plasmids from (**d**), and the mean number of puromycin-resistant colonies obtained per well (right). N=3 independent transfections; error bars, ±SEM.*

Figure 4

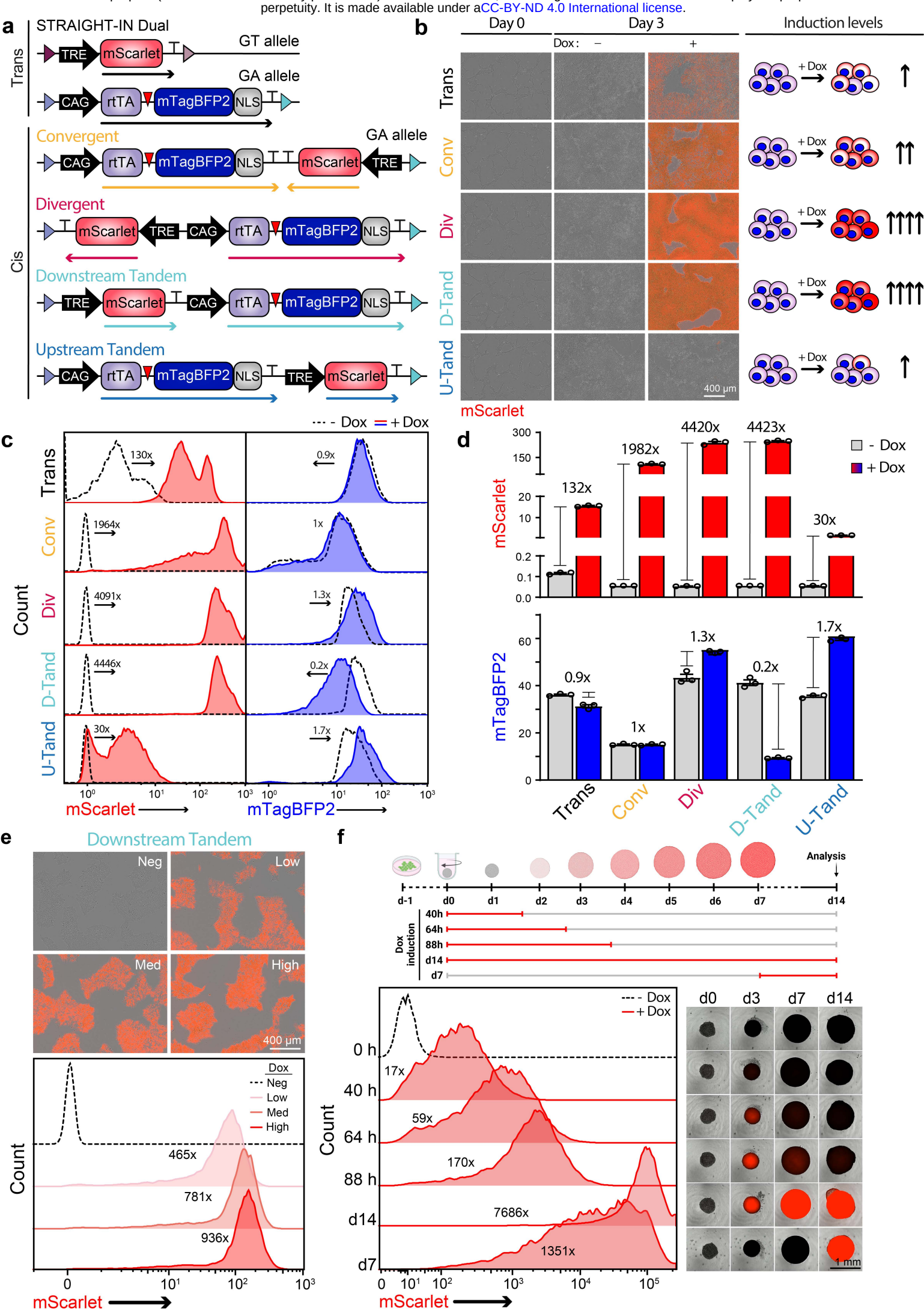

We also generated *cis* designs of the Tet-On 3G system, where both the constitutive (*rtTA-2A-mTagBFP2-NLS*) and inducible (*mScarlet*) transcriptional units were integrated into the same allele. This allowed us to investigate how gene syntax, specifically the relative orientation and order of the transcriptional units, affects induction. We created four possible syntaxes: convergent, divergent, downstream tandem and upstream tandem (**Figure 4a**). As the auxiliary sequences remaining in the GA allele could confound potential interactions between the constitutive and inducible genes, we examined mTagBFP2 and mScarlet expression both before (**Supplementary Figure 3**) and after excision of the sequences (**Figure 4**).
In the *trans* configuration, induced mScarlet expression was weak, whereas several *cis* designs showed robust induction (**Figure 4b**), suggesting that spatial proximity between the constitutive and inducible genes improves expression in the Tet-On 3G system. Notably, *mTagBFP2* expression levels remained unchanged in the *trans* configuration, indicating that resource burden was not a limiting factor in induction (**Figure 4c,d**).

Prior to induction, we observed clear bimodality in mTagBFP2 expression for the convergent syntax, which was most pronounced in unexcised cells (**Supplementary Figure 3c**), and aligned with biophysical models of transcription (Johnstone & Galloway, 2022). In contrast, the other syntaxes exhibited unimodal mTagBFP2 expression, which remained stable upon induction with doxycycline (**Supplementary Figure 3c**). Interestingly, in pre-excised cells, induction resulted in slight repression of mTagBFP2 across all syntaxes (**Supplementary Figure 3d**). However, after excision, syntax-specific differences in mTagBFP2 expression emerged (**Figure 4c,d**). Most notably, the downstream tandem syntax exhibited an ~5-fold reduction in mTagBFP2 expression, while the convergent syntax showed no significant change. The divergent and upstream tandem syntaxes showed increased mTagBFP2 expression, in line with biophysical model predictions (**Figure 4c,d**).

Upon induction with doxycycline, striking syntax-specific differences also emerged in mScarlet expression. Although these differences became more pronounced after excision (**Figure 4b-d**), similar trends were observed before excision (**Supplementary Figure 3e,f**). The divergent and downstream tandem syntaxes resulted in strong mScarlet induction, while the convergent and upstream tandem syntaxes showed poorer induction. Characterized by weak, bimodal, or broad expression distribution. Interestingly, excision significantly improved induction for the convergent syntax, possibly due to the increased expression of mTagBFP2 and therefore rtTA. However, excision did not improve induction for the upstream tandem syntax (**Figure 4c,d**).

Figure 4. Gene syntax influences the Tet-On 3G inducible system in hiPSCs

(a) *Schematic of a trans design and the four possible syntaxes of the all-in-one Tet-On 3G system, defined by the relative orientation (colored arrows) and order of the inducible (mScarlet) and constitutive (rtTA-2A-mTagBFP2) genes.*

(b) *Overlaid fluorescence and phase contrast images (left) of hiPSCs expressing inducible mScarlet from the constructs in (a), in the absence (-) and presence (+) of doxycycline; and a schematic (right) indicating relative mScarlet expression levels.*

(c) *Flow cytometric analysis of mScarlet and mTagBFP2 expression from the constructs in (a), in the absence (dashed line) or presence (red/blue) of doxycycline. Values indicate fold change based on the G-mean values.*

(d) *Mean G-mean values of mScarlet and mTagBFP2 expression from the constructs in (a), in the absence (grey) or presence (red/blue) of doxycycline. Fold change is based on the mean G-mean values. N=3 biological replicates; error bars, ±SEM.*

(e) *Overlaid fluorescence and phase contrast images (top) and flow cytometric analysis (bottom) of hiPSCs containing the downstream tandem syntax in (a), in the absence (dashed line) or presence (red) of varying doxycycline concentrations. Values in flow cytometric plots indicate fold change based on the G-mean values.*

(f) *Schematic of the cardioid differentiation protocol (top), flow cytometric analysis (bottom left), and overlaid fluorescence and phase contrast images (bottom right) of cardioids cultured in the absence (dashed line) or presence (red) of doxycycline for the indicated periods. Fold change values (x) are based on the G-mean values relative to untreated cardioids.*

Given the robust mScarlet induction observed in the downstream tandem *cis* design, we further explored its utility in 3D stem cell-derived structures such as cardiac organoids (i.e., cardioids), which provide more complex cellular environments for disease modeling and developmental studies. We found that mScarlet expression could be modestly adjusted by varying doxycycline concentration (**Figure 4e**). Additionally, altering the duration of doxycycline treatment modulated mScarlet expression, with longer inductions leading to higher expression (**Figure 4f**). Remarkably, even in developed cardioids, robust mScarlet expression could be achieved when adding doxycycline from day 7, demonstrating the potential to dynamically modulate gene dosage also in 3D organoids.

Dual inducible systems for forward programming and functional monitoring in hiPSCs

Forward programming drives hiPSCs into specific cell identities by overexpressing transcription factors. Potentially, suboptimal gene syntax may limit sufficient expression of the transcription factor. Thus, poor syntax may inhibit forward programming and fail to induce the new cell fate (**Figure 5a**). Given the striking differences we observed between the two tandem orientations (**Figure 4d**), we investigated whether the gene syntax influenced forward programming outcomes when overexpressing *Ngn2,* a pioneering transcription factor for neurons (Y. Zhang et al., 2013). To evaluate this, we constructed Tet-On 3G all-in-one systems for regulating Ngn2 expression using either the downstream or upstream tandem syntaxes.

Induction of *Ngn2* from the downstream tandem syntax led to the rapid generation of TUJ1+ and MAP2+ hiPSC-derived neurons within 7 days (**Figure 5b**, **Supplementary Figure 4a**). In contrast, almost no neurons were generated using the upstream tandem orientation syntax (**Figure 5c**). Based on our previous observation of poor *mScarlet* expression in the upstream tandem configuration, we hypothesize that limited Ngn2 expression in this orientation impairs forward programming. Indeed, qPCR analysis confirmed weaker induction of *Ngn2* and other neuronal genes in the upstream tandem syntax compared to the downstream tandem. As expected, pluripotency-associated genes were downregulated in the downstream tandem orientation after doxycycline induction (**Figure 5d**).

To demonstrate the utility of two orthogonal LPs, we used STRAIGHT-IN Dual to simultaneously overexpress Ngn2 and the genetically-encoded calcium indicator jRCaMP1b using the Tet-On 3G system. Each *CLYBL* allele harbored one of these transgene constructs under the control of a TRE (**Figure 5e**). With a single inducer, we achieved rapid and robust forward programming of hiPSCs into neurons while simultaneously recording calcium signals (**Figure 5f,g**, **Supplementary Figure 4b**).

Additionally, we designed a downstream tandem all-in-one Tet-On 3G GT donor plasmid to facilitate rapid cloning of genes of interest (GOIs), which also constitutively expresses a nuclear-localized BFP reporter (**Supplementary Figure 4c**). A LacZ cassette was included in the cloning site to enable easy blue/white screening of bacterial colonies that contained the cloned GOIs. After assembly, most white colonies (>85%) carried the correct cargo (**Supplementary Figure 4c,d**). This streamlined cloning and screening approach allowed for the rapid generation of donor plasmids with diverse inducible cargoes that could then be integrated using the rapid protocol into the STRAIGHT-IN alleles. These hiPSC lines, which were established in under one week, also uniformly expressed the nuclear BFP reporter (**Supplementary Figure 4e,f**).

To achieve independent control over two separate cargoes, we characterized an alternative inducible system in hiPSCs that, in combination with the Tet-On 3G system, would permit temporally and sequentially regulated expression of the distinct payloads. For this, we selected synthetic zinc finger transcription regulators (synZiFTRs) with ZF10 as the DNA-binding module, NS3 as the grazoprevir (GZV)-inducible module, and p65 as

Figure 5

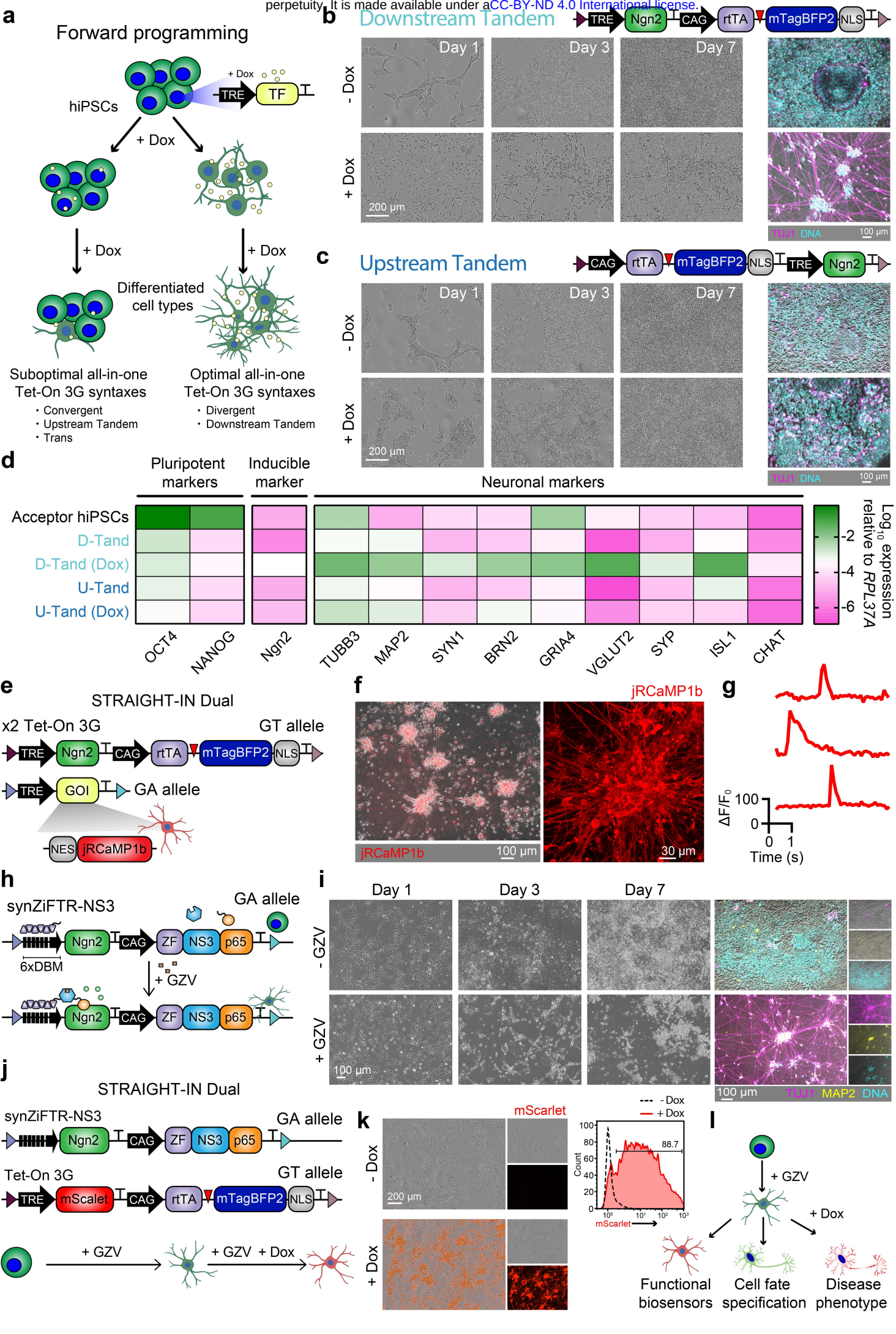

the transcriptional activator module (H.-S. Li et al., 2022). An all-in-one synZiFTR-based GZV-inducible GA donor plasmid was constructed based on the downstream tandem orientation (**Supplementary Figure 5a**). Induction of a *mGreenLantern* reporter with GZV revealed some toxicity, so we optimized the GZV concentration to achieve induction with minimal toxicity (**Supplementary Figure 5b,c**). Overexpression of Ngn2 using the GZV-inducible synZiFTR system successfully directed forward programming of hiPSCs into neurons within 7 days (**Figure 5h,i**).

Finally, we combined both inducible systems using STRAIGHT-IN Dual. Ngn2 was overexpressed via the all-in-one GZV-inducible synZiFTR system integrated into the GA allele, while mScarlet expression was induced using the all-in-one Tet-On 3G system targeted to the GT allele (**Figure 5j**). Remarkably, most neurons expressed mScarlet (**Figure 5k**, **Supplementary Figure 5d**).

These findings demonstrate the power and flexibility of dual inducible systems for precise control of transcription factor expression and functional monitoring. They also underscore the suitability of STRAIGHT-IN for rapidly evaluating the effects of different genetic syntaxes on these processes.

Discussion

In this study, we present STRAIGHT-IN Dual, a platform that enables the integration of two independent DNA payloads into the *CLYBL* locus with unprecedented allele-specific control, efficiency, and speed. Following protocol optimization, genetically modified hiPSC lines could be generated in less than one week with near 100% efficiency. For the GA allele, both integration and excision procedures could be completed within 9 days without the need to passage the cells.

Figure 5. Dual inducible expression of payloads using STRAIGHT-IN Dual

(a) *Schematic of the forward programming approach to differentiate hiPSCs into specific cell types by inducible overexpression of transcription factors.*

(b) *Schematic of the downstream tandem syntax for a doxycycline-inducible Ngn2 cassette (top). Phase contrast and immunofluorescence images (TUJ1, magenta; DNA, cyan) are of cells at different time points, cultured in the absence (-) or presence (+) of doxycycline (bottom).*

(c) *Schematic of the upstream tandem syntax for a doxycycline-inducible Ngn2 cassette (top). Phase contrast and immunofluorescence images (TUJ1, magenta; DNA, cyan) are of cells at different time points, cultured in the absence (-) or presence (+) of doxycycline (bottom).*

(d) *Gene expression analysis of pluripotency and neuronal markers in untransfected hiPSCs and cells containing the doxycycline-inducible Ngn2 cassettes from **(b)** or **(c)**, cultured in the absence or presence of doxycycline.*

(e) *Schematic of STRAIGHT-IN Dual hiPSCs containing the doxycycline-inducible Ngn2 cassette from **(b)** in the GT allele, and a doxycycline-inducible calcium indicator (jRCaMP1b) cassette in the GA allele.*

(f) *Overlaid fluorescence and phase contrast images (left), and fluorescence images (right) of forward programmed hiPSC-neurons expressing jRCaMP1b.*

(g) *Representative cytosolic Ca^{2+} transients recorded from day 7 forward programmed hiPSC-neurons.*

(h) *Schematic of a downstream tandem GZV-inducible (synZiFTR-NS3) Ngn2 cassette in the GA allele.*

(i) *Phase contrast and immunofluorescence images (TUJ1, magenta; MAP2, yellow; DNA, cyan) of cells at different time points, cultured in the absence (-) or presence (+) of GZV.*

(j) *Schematic of STRAIGHT-IN Dual hiPSCs containing a downstream tandem doxycycline-inducible mScarlet cassette in the GT allele, and the GZV-inducible Ngn2 cassette from **(h)** in the GA allele, and the sequential overexpression of these inducible transgenes using doxycycline and grazoprevir.*

(k) *Fluorescence and phase contrast images (left), and flow cytometric analysis (right) of forward programmed hiPSC-neurons after culturing in the absence (dashed line) or presence (red line) of doxycycline and grazoprevir.*

(l) *Schematic of a proposed sequential induction process to first direct hiPSCs to differentiate into neurons using the GZV-inducible synZiFTR system, followed by the doxycycline-inducible Tet-On 3G system for precise temporal overexpression of functional biosensors, transcription factors to further drive cell fate commitment, or dominant-negative genetic mutations to model neurological disorders.*

STRAIGHT-IN Dual allows for the simultaneous integration of two payloads with orthogonal precision due to the high specificity of the GT and GA sites (Jusiak et al., 2019). By using eeBxb1, a hyperactive Bxb1 mutant generated through directed evolution (Hew et al., 2024; Pandey et al., 2024), we could achieve significantly higher integration rates compared to Bxb1-WT. Since Bxb1 catalyzes recombination through DNA double-strand breaks (Xu et al., 2013), we also investigated the use of p53DD, a dominant-negative truncated version of p53, to dampen the p53-mediated DNA damage response and thereby increase the number of cells that proceed through the cell cycle after recombination (Haideri et al., 2024; M. Li et al., 2022; Rosenstein et al., 2024). By co-delivering eeBxb1 and p53DD as modRNA, we increased integration efficiency by approximately 10-fold, likely due to the improved survival of the hiPSCs following recombination.

The platform also provides near-scarless targeting of DNA payloads by enabling the excision of auxiliary elements, such as reporters, selection markers and plasmid backbones. Both here and in previous work (Blanch-Asensio et al., 2024), we have demonstrated that removing these flanking sequences reduces silencing of integrated payloads in both undifferentiated and differentiated hiPSCs. Excision also allows for the reuse of the selection markers for further genomic modifications. With STRAIGHT-IN Dual, we achieved nearly 100% efficiency in excising the auxiliary elements from both alleles using Cre and *Flp-2A-BleoR* modRNA, with the entire process for the GA allele possible without needing to replate the cells. This streamlined approach supports the seamless generation of multiple genetically modified hiPSC lines, either in parallel or pooled, potentially facilitating large-scale plasmid library integration and combinatorial studies at single-copy resolution. These optimized processes also make STRAIGHT-IN Dual highly compatible with automation pipelines, providing a robust platform for high-throughput generation of hiPSC lines for large-scale studies and functional screens.

Our results also highlight the limitations of current molecular tools used in hiPSCs. For example, the hEF1a promoter, despite its frequent use in synthetic biology and stem cell research, was rapidly silenced in hiPSCs after just a few passages, consistent with findings from other studies (Bertero et al., 2016). In contrast, the CAG] promoter provided robust, consistent gene expression in hiPSCs. However, its length and high GC content make it less desirable for cloning and use in hiPSCs. While this is not a limiting factor when using STRAIGHT-IN, there remains a need to identify additional promoters that resist silencing in hiPSCs. STRAIGHT-IN Dual offers a platform for rapid, locus-controlled screening of libraries containing novel or synthetic promoter sequences. Furthermore, transgene silencing frequently occurs during differentiation (Cabrera et al., 2022; Karbassi et al., 2024; Klatt et al., 2020; Rosenstein et al., 2024). Screening libraries of insulators or anti-silencing elements that perform effectively in both undifferentiated and differentiated hiPSCs would be invaluable for overcoming these challenges.

To demonstrate the utility of STRAIGHT-IN Dual for such screens, we compared the four gene syntaxes of the popular Tet-On 3G all-in-one inducible system in hiPSCs, finding that divergent and downstream tandem orientations provided optimal transgene expression. Additionally, placing inducible and constitutive transgenes on separate alleles generally resulted in lower induction levels compared to all-in-one designs. Most studies reporting the use of all-in-one Tet-On systems in mammalian cells have favored these two orientations (Jillette et al., 2019; Kelkar et al., 2020; Ng et al., 2021; Otomo et al., 2023; Randolph et al., 2017), with convergent and upstream tandem syntaxes typically performing poorly unless extensively optimized (Haenebalcke et al., 2013; Shin et al., 2024).

Based on the clear differences in expression observed in the two tandem orientations, we evaluated both syntaxes for forward programming of hiPSCs into neurons via inducible expression of Ngn2. We selected the downstream tandem syntax

over the divergent orientation because we observed higher transgene induction prior to excision of the flanking auxiliary elements, thereby obviating the need to perform this step and allowing for the initiation of overexpression studies within one week. Remarkably, forward programming was only effective in generating functional neurons when using the downstream tandem syntax, confirming its superior performance over the upstream tandem syntax.

This system opens new avenues for screening transcription factors that drive the differentiation of hiPSCs into specific cell types. Previously, such screens were only achievable using viral-based strategies (Joung et al., 2023; Ng et al., 2021). With STRAIGHT-IN, transcription factor libraries could be screened in a similar timeframe, but with locus-specific and precise single-copy control, which is not possible with viral methods.

Moreover, STRAIGHT-IN Dual allows for combinatorial or sequential transgene overexpression using independent inducible systems, such as Tet-On 3G, and synZiFTRs. We demonstrated this using the grazoprevir-inducible synZiFTR system to overexpress *Ngn2* in hiPSCs, followed by mScarlet expression via the Tet-On 3G system in the resulting neurons. Surprisingly, we observed some toxicity with grazoprevir in hiPSCs, a phenomenon not reported in more terminally differentiated human cell types, such as primary T cells (H.-S. Li et al., 2022).

By combining multiple inducible systems, specific cell fate engineering along with the expression of functional biosensors or the modeling of sporadic or acquired genetic mutations in differentiated cells, is now be possible (**Figure 5I**). Furthermore, these inducible DNA payloads can be expressed in complex in vitro cell models, providing a powerful tool for bioengineering in organoids, organs-on-chips, and other 3D *in vitro* cultures (Nahon et al., 2024). In summary, STRAIGHT-IN Dual facilitates the rapid generation of complex genetically modified hiPSC lines, and we envision that this technology will become a valuable tool for hiPSC research and biomedicine.

Acknowledgements

We thank Niels Geijsen and Peng Shang for providing Cre protein. Some schematics in figures were created with BioRender.com. This work was supported by the Netherlands Organ-on-Chip Initiative, a Nederlandse Organisatie voor Wetenschappelijk Onderzoek (NWO) Gravitation project funded by the Ministry of Education, Culture, and Science of the government of the Netherlands (024.003.001), a ZonMw PSIDER consortium grant (no. 10250022120002; GREAT). This work is also part of the project “Innovative Stem Cell Technology Infrastructure for human organ and disease models” (no. 184.036.006 of the research program Large-scale research infrastructure which is financed by NWO). The Novo Nordisk Foundation Center for Stem Cell Medicine (reNEW) is supported by a Novo Nordisk Foundation grant (NNF21CC0073729). Research reported in this manuscript was supported by the National Institute of General Medical Sciences of the National Institutes of Health under award number R35-GM143033 (K.E.G), by the National Science Foundation under the NSF-CAREER under award number 2339986, and with funding from Institute for Collaborative Biotechnologies.

Author contributions

A.B-A developed and optimized the protocols described in this manuscript, designed and performed the experiments, analyzed the data and wrote the manuscript. D.S.P developed and optimized some of the protocols described in this manuscript, designed and performed some of the experiments, contributed to drafting the manuscript and revised it for important intellectual content. N.B.W designed and performed some of the experiments, contributed to drafting the manuscript and revised it for important intellectual content. C.L.M acquired some of the funding and revised the manuscript for important intellectual content. K.E.G and R.P.D. supervised the study, acquired some of the funding and revised the manuscript for important intellectual content. All authors approved the final manuscript.

References

- Anzalone, A. V., Gao, X. D., Podracky, C. J., Nelson, A. T., Koblan, L. W., Raguram, A., Levy, J. M., Mercer, J. A. M., & Liu, D. R. (2022). Programmable deletion, replacement, integration and inversion of large DNA sequences with twin prime editing. *Nature Biotechnology*, *40*(5), 731–740. https://doi.org/10.1038/s41587-021-01133-w
- Balmas, E., Sozza, F., Bottini, S., Ratto, M. L., Savorè, G., Becca, S., Snijders, K. E., & Bertero, A. (2023). Manipulating and studying gene function in human pluripotent stem cell models. *FEBS Letters*, *597*(18), 2250–2287. https://doi.org/10.1002/1873-3468.14709
- Bertero, A., Pawlowski, M., Ortmann, D., Snijders, K., Yiangou, L., De Brito, M. C., Brown, S., Bernard, W. G., Cooper, J. D., Giacomelli, E., Gambardella, L., Hannan, N. R. F., Iyer, D., Sampaziotis, F., Serrano, F., Zonneveld, M. C. F., Sinha, S., Kotter, M., & Vallier, L. (2016). Optimized inducible shRNA and CRISPR/Cas9 platforms for in vitro studies of human development using hPSCs. *Development*, *143*(23), 4405–4418. https://doi.org/10.1242/dev.138081
- Blanch-Asensio, A., Grandela, C., Brandão, K. O., de Korte, T., Mei, H., Ariyurek, Y., Yiangou, L., Mol, M. P. H., van Meer, B. J., Kloet, S. L., Mummery, C. L., & Davis, R. P. (2022). STRAIGHT-IN enables high-throughput targeting of large DNA payloads in human pluripotent stem cells. *Cell Reports Methods*, *2*(10), 100300. https://doi.org/10.1016/J.CRMETH.2022.100300
- Blanch-Asensio, A., Grandela, C., Mummery, C. L., & Davis, R. P. (2024). STRAIGHT-IN: a platform for rapidly generating panels of genetically modified human pluripotent stem cell lines. *Nature Protocols*. https://doi.org/10.1038/s41596-024-01039-2
- Blanch-Asensio, A., Vaart, B. Van Der, Vinagre, M., Groen, E., Arendzen, C., Freund, C., Geijsen, N., Mummery, C. L., & Davis, R. P. (2023). Generation of AAVS1 and CLYBL STRAIGHT-IN v2 acceptor human iPSC lines for integrating DNA payloads. *Stem Cell Research*, *66*, 102991. https://doi.org/10.1016/j.scr.2022.102991
- Brandão, K. O., Brink, L. van den, Miller, D. C., Grandela, C., van Meer, B. J., Mol, M. P. H., de Korte, T., Tertoolen, L. G. J., Mummery, C. L., Sala, L., Verkerk, A. O., & Davis, R. P. (2020). Isogenic Sets of hiPSC-CMs Harboring Distinct KCNH2 Mutations Differ Functionally and in Susceptibility to Drug-Induced Arrhythmias. *Stem Cell Reports*, *15*(5), 1127–1139. https://doi.org/10.1016/j.stemcr.2020.10.005
- Brosh, R., Laurent, J. M., Ordoñez, R., Huang, E., Hogan, M. S., Hitchcock, A. M., Mitchell, L. A., Pinglay, S., Cadley, J. A., Luther, R. D., Truong, D. M., Boeke, J. D., & Maurano, M. T. (2021). A versatile platform for locus-scale genome rewriting and verification. *Proceedings of the National Academy of Sciences of the United States of America*, *118*(10), 1–11. https://doi.org/10.1073/pnas.2023952118
- Brown, W. R. A., Lee, N. C. O., Xu, Z., & Smith, M. C. M. (2011). Serine recombinases as tools for genome engineering. *Methods*, *53*(4), 372–379. https://doi.org/10.1016/j.ymeth.2010.12.031
- Cabrera, A., Edelstein, H. I., Glykofrydis, F., Love, K. S., Palacios, S., Tycko, J., Zhang, M., Lensch, S., Shields, C. E., Livingston, M., Weiss, R., Zhao, H., Haynes, K. A., Morsut, L., Chen, Y. Y., Khalil, A. S., Wong, W. W., Collins, J. J., Rosser, S. J., … Deans, T. L. (2022). The sound of silence: Transgene silencing in mammalian cell engineering. *Cell Systems*, *13*(12), 950–973. https://doi.org/10.1016/j.cels.2022.11.005
- Dou, Y., Lin, Y., Wang, T. yun, Wang, X. Y., Jia, Y. long, & Zhao, C. peng. (2021). The CAG promoter maintains high-level transgene expression in HEK293 cells. *FEBS Open Bio*, *11*(1), 95–104. https://doi.org/10.1002/2211-5463.13029
- Duportet, X., Wroblewska, L., Guye, P., Li, Y., Eyquem, J., Rieders, J., Rimchala, T., Batt, G., & Weiss, R. (2014). A platform for rapid prototyping of synthetic gene networks in mammalian cells. *Nucleic Acids Research*, *42*(21), 13440–13451. https://doi.org/10.1093/nar/gku1082
- Durrant, M. G., Fanton, A., Tycko, J., Hinks, M., Chandrasekaran, S. S., Perry, N. T., Schaepe, J., Du, P. P., Lotfy, P., Bassik, M. C., Bintu, L., Bhatt, A. S., & Hsu, P. D. (2023). Systematic discovery of recombinases for efficient integration of large DNA sequences into the human genome. *Nature Biotechnology*, *41*, 488–499. https://doi.org/10.1038/s41587-022-01494-w
- Engreitz, J. M., Haines, J. E., Perez, E. M., Munson, G., Chen, J., Kane, M., McDonel, P. E., Guttman, M., & Lander, E. S. (2016). Local regulation of gene expression by lncRNA promoters, transcription and splicing. *Nature*, *539*(7629), 452–455. https://doi.org/10.1038/nature20149
- Haenebalcke, L., Goossens, S., Dierickx, P., Bartunkova, S., D'Hont, J., Haigh, K., Hochepied, T., Wirth, D., Nagy, A., & Haigh, J. J. (2013). The ROSA26-iPSC Mouse: A Conditional, Inducible, and Exchangeable Resource for Studying Cellular (De)Differentiation. *Cell Reports*, *3*(2), 335–341. https://doi.org/10.1016/j.celrep.2013.01.016
- Haideri, T., Howells, A., Jiang, Y., Yang, J., Bao, X., & Lian, X. L. (2022). Robust genome editing via modRNA-based Cas9 or base editor in human pluripotent stem cells. *Cell Reports Methods*, *2*(9), 100290. https://doi.org/10.1016/j.crmeth.2022.100290
- Haideri, T., Lin, J., Bao, X., & Lian, X. L. (2024). MAGIK: A rapid and efficient method to create lineage-specific reporters in human pluripotent stem cells. *Stem Cell Reports*, *19*(5), 744–757. https://doi.org/10.1016/j.stemcr.2024.03.005
- Hew, B. E., Gupta, S., Sato, R., Waller, D. F., Stoytchev, I., Short, J. E., Sharek, L., Tran, C. T., Badran, A. H., & Owens, J. B. (2024). Directed evolution of hyperactive integrases for site specific insertion of transgenes. *Nucleic Acids Research*, *52*(14), e64. https://doi.org/10.1093/nar/gkae534
- Hosur, V., Low, B. E., & Wiles, M. V. (2022). Programmable RNA-Guided Large DNA Transgenesis by CRISPR/Cas9 and Site-Specific Integrase Bxb1. *Frontiers in Bioengineering and Biotechnology*, *10*, 910151. https://doi.org/10.3389/fbioe.2022.910151

- Jelicic, M., Schmitt, L. T., Paszkowski-Rogacz, M., Walder, A., Schubert, N., Hoersten, J., Sürün, D., & Buchholz, F. (2023). Discovery and characterization of novel Cre-Type tyrosine site-specific recombinases for advanced genome engineering. *Nucleic Acids Research*, *51*(10), 5285–5297. https://doi.org/10.1093/nar/gkad366
- Jillette, N., Du, M., Zhu, J. J., Cardoz, P., & Cheng, A. W. (2019). Split selectable markers. *Nature Communications*, *10*, 4968. https://doi.org/10.1038/s41467-019-12891-2
- Johnstone, C. P., & Galloway, K. E. (2022). Supercoiling-mediated feedback rapidly couples and tunes transcription. *Cell Reports*, *41*(3), 111492. https://doi.org/10.1016/j.celrep.2022.111492
- Joung, J., Ma, S., Tay, T., Geiger-Schuller, K. R., Kirchgatterer, P. C., Verdine, V. K., Guo, B., Arias-Garcia, M. A., Allen, W. E., Singh, A., Kuksenko, O., Abudayyeh, O. O., Gootenberg, J. S., Fu, Z., Macrae, R. K., Buenrostro, J. D., Regev, A., & Zhang, F. (2023). A transcription factor atlas of directed differentiation. *Cell*, *186*(1), 209–229. https://doi.org/10.1016/j.cell.2022.11.026
- Jusiak, B., Jagtap, K., Gaidukov, L., Duportet, X., Bandara, K., Chu, J., Zhang, L., Weiss, R., & Lu, T. K. (2019). Comparison of Integrases Identifies Bxb1-GA Mutant as the Most Efficient Site-Specific Integrase System in Mammalian Cells. *ACS Synthetic Biology*, *8*(1), 16–24. https://doi.org/10.1021/acssynbio.8b00089
- Karbassi, E., Padgett, R., Bertero, A., Reinecke, H., Klaiman, J. M., Yang, X., Hauschka, S. D., & Murry, C. E. (2024). Targeted CRISPR activation is functional in engineered human pluripotent stem cells but undergoes silencing after differentiation into cardiomyocytes and endothelium. *Cellular and Molecular Life Sciences*, *81*(1), 95. https://doi.org/10.1007/s00018-023-05101-2
- Kelkar, A., Zhu, Y., Groth, T., Stolfa, G., Stablewski, A. B., Singhi, N., Nemeth, M., & Neelamegham, S. (2020). Doxycycline-Dependent Self-Inactivation of CRISPR-Cas9 to Temporally Regulate On- and Off-Target Editing. *Molecular Therapy*, *28*(1), 29–41. https://doi.org/10.1016/j.ymthe.2019.09.006
- Klatt, D., Cheng, E., Hoffmann, Di., Santilli, G., Thrasher, A. J., Brendel, C., & Schambach, A. (2020). Differential Transgene Silencing of Myeloid-Specific Promoters in the AAVS1 Safe Harbor Locus of Induced Pluripotent Stem Cell-Derived Myeloid Cells. *Human Gene Therapy*, *31*(3–4), 199–210. https://doi.org/10.1089/hum.2019.194
- Li, H.-S., Israni, D. V, Gagnon, K. A., Ann Gan, K., Raymond, M. H., Sander, J. D., Roybal, K. T., Keith Joung, J., Wong, W. W., & Khalil, A. S. (2022). Multidimensional control of therapeutic human cell function with synthetic gene circuits. *Science* , *378*(6625), 1227–1234. https://doi.org/10.1126/science.ade0156
- Li, J., Li, Y., Pawlik, K. M., Napierala, J. S., & Napierala, M. (2020). A CRISPR-Cas9, Crelox, and Flp-FRT Cascade Strategy for the Precise and Efficient Integration of Exogenous DNA into Cellular Genomes. *CRISPR Journal*, *3*(6), 470–486. https://doi.org/10.1089/crispr.2020.0042
- Li, M., Zhong, A., Wu, Y., Sidharta, M., Beaury, M., Zhao, X., Studer, L., & Zhou, T. (2022). Transient inhibition of p53 enhances prime editing and cytosine base-editing efficiencies in human pluripotent stem cells. *Nature Communications*, *13*(1), 6354. https://doi.org/10.1038/s41467-022-34045-7
- Low, B. E., Hosur, V., Lesbirel, S., & Wiles, M. V. (2022). Efficient targeted transgenesis of large donor DNA into multiple mouse genetic backgrounds using bacteriophage Bxb1 integrase. *Scientific Reports*, *12*, 5424. https://doi.org/10.1038/s41598-022-09445-w
- Matreyek, K. A., Stephany, J. J., & Fowler, D. M. (2017). A platform for functional assessment of large variant libraries in mammalian cells. *Nucleic Acids Research*, *45*(11), e102. https://doi.org/10.1093/nar/gkx183
- Mitchell, L. A., McCulloch, L. H., Pinglay, S., Berger, H., Bosco, N., Brosh, R., Bulajic, M., Huang, E., Hogan, M. S., Martin, J. A., Mazzoni, E. O., Davoli, T., Maurano, M. T., & Boeke, J. D. (2021). De novo assembly and delivery to mouse cells of a 101 kb functional human gene. *Genetics*, *218*(1), iyab038. https://doi.org/10.1093/genetics/iyab038
- Nahon, D. M., Moerkens, R., Aydogmus, H., Lendemeijer, B., Martínez-Silgado, A., Stein, J. M., Dostanić, M., Frimat, J.-P., Gontan, C., de Graaf, M. N. S., Hu, M., Kasi, D. G., Koch, L. S., Le, K. T. T., Lim, S., Middelkamp, H. H. T., Mooiweer, J., Motreuil-Ragot, P., Niggl, E., … Mummery, C. L. (2024). Standardizing designed and emergent quantitative features in microphysiological systems. *Nature Biomedical Engineering*, *8*(8), 941–962. https://doi.org/10.1038/s41551-024-01236-0
- Ng, A. H. M., Khoshakhlagh, P., Rojo Arias, J. E., Pasquini, G., Wang, K., Swiersy, A., Shipman, S. L., Appleton, E., Kiaee, K., Kohman, R. E., Vernet, A., Dysart, M., Leeper, K., Saylor, W., Huang, J. Y., Graveline, A., Taipale, J., Hill, D. E., Vidal, M., … Church, G. M. (2021). A comprehensive library of human transcription factors for cell fate engineering. *Nature Biotechnology*, *39*(4), 510–519. https://doi.org/10.1038/s41587-020-0742-6
- Otomo, J., Woltjen, K., & Sakurai, H. (2023). Uniform transgene activation in Tet-On systems depends on sustained rtTA expression. *IScience*, *26*(10), 107685. https://doi.org/10.1016/j.isci.2023.107685
- Pandey, S., Gao, X. D., Krasnow, N. A., McElroy, A., Tao, Y. A., Duby, J. E., Steinbeck, B. J., McCreary, J., Pierce, S. E., Tolar, J., Meissner, T. B., Chaikof, E. L., Osborn, M. J., & Liu, D. R. (2024). Efficient site-specific integration of large genes in mammalian cells via continuously evolved recombinases and prime editing. *Nature Biomedical Engineering*. https://doi.org/10.1038/s41551-024-01227-1
- Patel, H. P., Coppola, S., Pomp, W., Aiello, U., Brouwer, I., Libri, D., & Lenstra, T. L. (2023). DNA supercoiling restricts the transcriptional bursting of neighboring eukaryotic genes. *Molecular Cell*, *83*(10), 1573-1587.e8. https://doi.org/10.1016/j.molcel.2023.04.015
- Pawlowski, M., Ortmann, D., Bertero, A., Tavares, J. M., Pedersen, R. A., Vallier, L., & Kotter, M. R. N. (2017). Inducible and Deterministic Forward Programming of Human Pluripotent Stem Cells into Neurons, Skeletal Myocytes, and Oligodendrocytes. *Stem Cell Reports*, *8*(4), 803–812. https://doi.org/10.1016/j.stemcr.2017.02.016

- Peterman, E. L., Ploessl, D. S., & Galloway, K. E. (2024). Accelerating Diverse Cell-Based Therapies Through Scalable Design. *Annual Review of Chemical and Biomolecular Engineering*, *15*, 267–292. https://doi.org/10.1146/annurev-chembioeng
- Pinglay, S., Bulajić, M., Rahe, D. P., Huang, E., Brosh, R., Mamrak, N. E., King, B. R., German, S., Cadley, J. A., Rieber, L., Easo, N., Lionnet, T., Mahony, S., Maurano, M. T., Holt, L. J., Mazzoni, E. O., & Boeke, J. D. (2022). Synthetic regulatory reconstitution reveals principles of mammalian Hox cluster regulation. *Science* , *377*(6601), eabk2820. https://doi.org/10.1126/science.abk2820
- Randolph, L. N., Bao, X., Zhou, C., & Lian, X. (2017). An all-in-one, Tet-On 3G inducible PiggyBac system for human pluripotent stem cells and derivatives. *Scientific Reports*, *7*(1), 1549. https://doi.org/10.1038/s41598-017-01684-6
- Roelle, S. M., Kamath, N. D., & Matreyek, K. A. (2023). Mammalian Genomic Manipulation with Orthogonal Bxb1 DNA Recombinase Sites for the Functional Characterization of Protein Variants. *ACS Synthetic Biology*, *12*(11), 3352–3365. https://doi.org/10.1021/acssynbio.3c00355
- Rosenstein, A. H., Sambathkumar, R., Murareanu, B. M., Dhaliwal, N. K., Sun, F., Zhao, X., Dadvar, A., Al-Attar, R., Chai, A., Gulati, N., Yin, T., Nguyen, M., Serra, D., Devina, T., Gilbert, P., Kunath, T., Laflamme, M. A., Ogawa, S., Muffat, J., … Garton, M. (2024). FAST-STEM: A Human pluripotent stem cell engineering toolkit for rapid design-build-test-learn development of human cell-based therapeutic devices. *BioRxiv Published Online May 24, 2024.* https://doi.org/10.1101/2024.05.23.595541
- Seczynska, M., Bloor, S., Cuesta, S. M., & Lehner, P. J. (2022). Genome surveillance by HUSH-mediated silencing of intronless mobile elements. *Nature*, *601*(7893), 440–445. https://doi.org/10.1038/s41586-021-04228-1
- Shin, S. W., Min, H., Kim, J., & Lee, J. S. (2024). A Precise and Sustainable Doxycycline-Inducible Cell Line Development Platform for Reliable Mammalian Cell Engineering with Gain-of-Function Mutations. *Metabolic Engineering*. https://doi.org/10.1016/j.ymben.2024.09.004
- Xu, Z., Thomas, L., Davies, B., Chalmers, R., Smith, M., & Brown, W. (2013). Accuracy and efficiency define Bxb1 integrase as the best of fifteen candidate serine recombinases for the integration of DNA into the human genome. *BMC Biotechnology*, *13*, 1–17. https://doi.org/10.1186/1472-6750-13-87
- Yarnall, M. T. N., Ioannidi, E. I., Schmitt-Ulms, C., Krajeski, R. N., Lim, J., Villiger, L., Zhou, W., Jiang, K., Garushyants, S. K., Roberts, N., Zhang, L., Vakulskas, C. A., Walker, J. A., Kadina, A. P., Zepeda, A. E., Holden, K., Ma, H., Xie, J., Gao, G., … Gootenberg, J. S. (2023). Drag-and-drop genome insertion of large sequences without double-strand DNA cleavage using CRISPR-directed integrases. *Nature Biotechnology*, *41*, 500–512. https://doi.org/10.1038/s41587-022-01527-4
- Zhang, H., Lesnov, G. D., Subach, O. M., Zhang, W., Kuzmicheva, T. P., Vlaskina, A. V., Samygina, V. R., Chen, L., Ye, X., Nikolaeva, A. Y., Gabdulkhakov, A., Papadaki, S., Qin, W., Borshchevskiy, V., Perfilov, M. M., Gavrikov, A. S., Drobizhev, M., Mishin, A. S., Piatkevich, K. D., & Subach, F. V. (2024). Bright and stable monomeric green fluorescent protein derived from StayGold. *Nature Methods*, *21*(4), 657–665. https://doi.org/10.1038/s41592-024-02203-y
- Zhang, M., Yang, C., Tasan, I., & Zhao, H. (2021). Expanding the Potential of Mammalian Genome Engineering via Targeted DNA Integration. *ACS Synthetic Biology*, *10*(3), 429–446. https://doi.org/10.1021/acssynbio.0c00576
- Zhang, Y., Pak, C. H., Han, Y., Ahlenius, H., Zhang, Z., Chanda, S., Marro, S., Patzke, C., Acuna, C., Covy, J., Xu, W., Yang, N., Danko, T., Chen, L., Wernig, M., & Südhof, T. C. (2013). Rapid single-step induction of functional neurons from human pluripotent stem cells. *Neuron*, *78*(5), 785–798. https://doi.org/10.1016/j.neuron.2013.05.029
- Zhu, F., Gamboa, M., Farruggio, A. P., Hippenmeyer, S., Tasic, B., Schüle, B., Chen-Tsai, Y., & Calos, M. P. (2014). DICE, an efficient system for iterative genomic editing in human pluripotent stem cells. *Nucleic Acids Research*, *42*(5), e34. https://doi.org/10.1093/nar/gkt1290